JOURNAL OF Applied Polymer SCIENCE

Synthesis of PS-*g*-POSS Hybrid Graft Copolymer by Click Coupling via "Graft Onto" Strategy

Maoshan Niu, Tao Li, Riwei Xu, Xiaoyu Gu, Dingsheng Yu, Yixian Wu
State Key Laboratory of Chemical Resource Engineering, Key Laboratory of Carbon Fiber and Functional polymers (Ministry of Education), Beijing University of Chemical Technology, Beijing 100029, China
Correspondence to: R.W. Xu (E-mail: xurw@mail.buct.edu.cn); Y.X. Wu (E-mail: wuyx@mail.buct.edu.cn)

ABSTRACT: Polystyrene (PS)-incorporated polyhedral oligomeric silsesquioxanes (POSS) organic–inorganic hybrid graft copolymer could be achieved by click coupling reaction between alkyne groups in POSS and azido groups in PS via "graft onto" strategy. Alkyne-functionalized POSS was synthesized via thiol-ene facile click reaction and subsequent amidation reaction with very high yield. Azido-multifunctionalized PS could be synthesized by chloromethylation and subsequent azido reaction. The chemical structures of PS-$(CH_2Cl)_m$, PS-$(CH_2N_3)_m$, and PS-*g*-POSS were determined by Fourier transform infrared and ^{1}H NMR characterization. PS-*g*-POSS presented a better hydrophobic property with contact angle of 113° than that of PS (85°). And PS-*g*-POSS with ≤5% of grafting degree had lower glass transition temperature (T_g) than that of PS and then it increased up to 112°C with grafting degree. An obvious aggregation of POSS phase with 10–80 nm in size was formed in PS-*g*-POSS matrix. In addition, 5 wt % of PS-*g*-POSS was added to general purpose polystyrene (GPPS) to remarkably improve its tensile strength from 45 to 57 MPa. © 2012 Wiley Periodicals, Inc. J. Appl. Polym. Sci. 129: 1833–1844, 2013

KEYWORDS: functionalization of polymers; self-assembly; nanoparticles; nanowires and nanocrystals; grafting; polystyrene

Received 20 September 2012; accepted 25 November 2012; published online 24 December 2012
DOI: 10.1002/app.38877

INTRODUCTION

Organic–inorganic hybrid materials have been regarded as new generation of high performance materials since they combine the advantages of inorganic materials and organic polymers.[1,2] The formation of dispersed nanoparticles in polymeric matrices offers unique opportunities for designing advanced functional materials, and the formulation of high-performance polymer-based nanocomposites, for example, improved stiffness, dimensional stability, barrier properties, and fire retardancy, is a very promising and challenging issue from scientific and industrial point of view.[3–6] Generally, organic–inorganic hybrid materials can be prepared by physical blending or chemical reaction, and among those chemical synthetic approaches to obtain nanocomposites, the use of structurally well-defined inorganic nanoparticles or clusters becomes an increasingly important strategy.[7] Furthermore, the problem associated with microphase separation in organic–inorganic hybrid materials can be alleviated either through the nanoparticles being covalently bound to a polymer backbone or modification of their surface properties.[8]

Polystyrene (PS), one of the largest commercial polymers, has a relatively low glass transition temperature (T_g), brittleness, and wettability, which have limited their further applications in several situations.[9] In this few years, polyhedral oligomeric silsesquioxanes (POSS)/PS composites are prepared and aimed to improve various performances of PS.[10,11] POSS are particularly a type of model nanostructured hybrid materials that provide a better choice to form nanocomposites. A typical POSS molecule has a cage-like inorganic core in the range of a nanometer, surrounded by organic corner groups, which endow the POSS molecule with a higher solubility in organic solvents and reactivity.[12,13] In addition, because of nanometer size effect and steric hindrance, POSS derivatives have been shown to increase the glass transition temperature, modulus, and oxygen permeability when incorporated into polymer matrices.[14,15] Moreover, with a good designability of POSS structure, it can be incorporated into PS via either copolymerization, grafting reaction, or other methods. A "plug and play" polymer[16] was prepared with hydrogen-bonding recognition between diamidopyridine-functionalized POSS and thymine-functionalized PS, and thermal characterization of the nanocomposites effectively demonstrates the advantages of POSS crystallinity and the overall benefits of multiple hydrogen-bonding interactions within polymer systems. A series of PS-based random copolymers[17] bearing POSS moieties with varying vertex group (isobutyl, cyclopentyl, and cyclohexyl) composition were synthesized, and the influence factors of intermolecular interactions and free volume on glass transition temperature were discussed. The preparation of styrene/

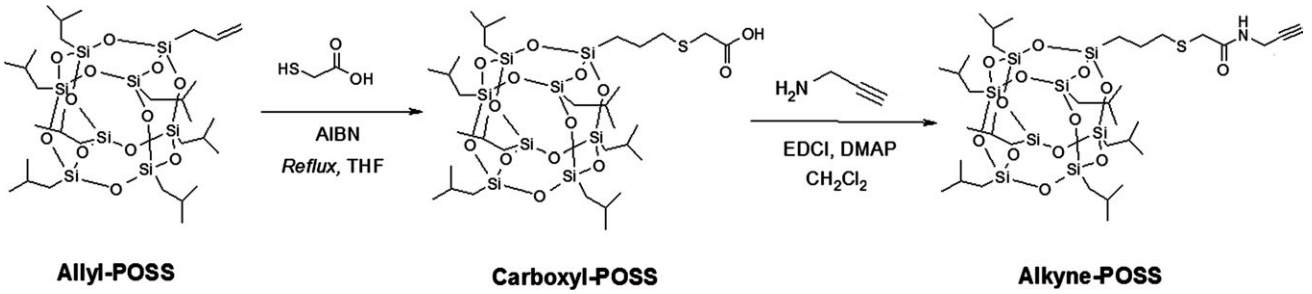

Scheme 1. Synthesis of alkyne-functionalized polyhedral oligomeric silsesquioxanes (alkyne-POSS).

styryl-POSS hybrid copolymer[18] with $CpTiCl_3$ as initiator was reported, and the experimental results indicate that the T_g of copolymers increased from 97 to 105°C for 0–4.5 mol % styryl-POSS content. However, most of the POSS covalently linked PS composites were synthesized by polymerization with styryl-POSS, which might be costly for application. Meanwhile, because of the steric effect of POSS, the efficiency is not high, such as the reaction time would last for 2 days by free radical polymerization in the presence of azodiisobutyronitrile (AIBN) as a radical initiator,[17] or the molecular weight of products and polydispersity index (PDI) in the range 2–6 could not be controlled well in general.[18]

Nowadays, more attention has focused on a higher efficient way to prepare hybrid materials, and the click chemistry reaction with equimolarity, high yields, and so on[19,20] attract more and more attention. With the purpose of "click" active functional group, it needs to further design and synthesize functional POSS, such as mono-azidohydrinisobutyl POSS[21] and octakis (3-azidopropyl) POSS, respectively,[22] and lot of other functional POSS derivatives have been synthesized by corner-capping reactions, substitution reaction with retention of the siloxane cage, and so on summarized at large in review.[23] With the click chemistry, the linear- and star-shaped telechelic POSS-containing hybrid PS were prepared by Huisgen cycloaddition reaction of alkyne-functionalized POSS (alkyne-POSS) with monochelic and telechelic azido-terminated PS.[24]

In this article, we describe a facile method to prepare PS-*g*-POSS graft hybrid copolymer by click chemistry between monofunctional alkyne-POSS and multifunctional azido-PS. First, alkyne-POSS is synthesized with high efficiency via thiol-ene click reaction and further amidation reaction with propargylamine. Second, PS was chemically modified by chloromethylation and subsequent azido reduction to synthesize PS-$(CH_2N_3)_m$. Alkyne-POSS was grafted onto PS-$(CH_2N_3)_m$ via Cu (I)-catalyzed 1,3-dipolarcycloaddition. The structures and thermal properties of PS-*g*-POSS were further studied in detail. Third, the self-assemble behavior of PS-*g*-POSS and mechanical properties of GPPS/PS-*g*-POSS composites were also discussed.

EXPERIMENTAL

Materials

The commercial general purpose PS (GPPS) with number molecular weight (M_n) of 93 × 10^3 g/mol and PDI of 2.4 was supplied from Beijing Yanshan Petrochemical, China. Other PS samples (PS-13k, PS-38k, and PS-110k) were synthesized in our laboratory by anionic polymerization with M_n of 13 × 10^3, 38 × 10^3, and 110 × 10^3 g/mol, respectively, and PDI of 1.1. Allyl isobutyl POSS (allyl-POSS) was purchased from Hybrid Plastics Company (USA). 1,3,5-Trioxane (Alfa Aesar, Ward Hill, MA, USA), chlorotrimethylsilane [TMCS; Sinopharm Chemical Reagent Co., Ltd. (SCRC)], tin(IV) chloride ($SnCl_4$, SCRC), sodium azide (NaN_3; Alfa Aesar), thioglycolic acid (SCRC), 2-propynylamine (SCRC), 4-dimethylamiopyridine (DMAP; Alfa Aesar), *N*-ethyl-*N*′-(3-dimethylaminopropyl) carbodiimide hydrochloride (EDCI.HCl; Alfa Aesar), copper iodide (CuI, SCRC), and *N*,*N*,*N*′,*N*′,*N*″-pentamethyldiethylenetriamine (PMDETA; Alfa Aesar) were used as received. AIBN (SCRC) was recrystallized from methanol.

Synthesis

Synthesis of Carboxyl-Functionalized POSS (Carboxyl-POSS). Carboxyl-functionalized POSS (carboxyl-POSS) with near complete yield was synthesized via thiol-ene reaction of allyl-isobutyl POSS with thioglycolic acid (Scheme 1). Typically, allyl-isobutyl POSS (5 g, 5.83 mmol) and thioglycolic acid (2.02 mL, 29.15 mmol) were dissolved in 20 mL of tetrahydrofuran (THF) in a flask, and then AIBN (0.5 g, 0.3 mmol) was added under nitrogen. Then, thiol-ene reaction was conducted at 80°C for 6 h. The reaction mixture was precipitated in acetonitrile at room temperature. The resulting 5.41 g of carboxyl-functionalized POSS was dried at 50°C overnight and then characterized by Fourier transform infrared (FTIR) (KBr, cm^{-1}) and ^{1}H NMR. FTIR: 1110 (Si—O—Si), 1711 (C=O); ^{1}H-NMR ($CDCl_3$, 400 MHz, δ ppm): 3.27 (s, 2H, —S—C***H*****$_2$**—CO—), 2.71–2.67 (m, 2H, —CH_2—C***H*****$_2$**—S—), 1.74 (t, 2H, —Si—CH_2—C***H*****$_2$**—CH_2—), 0.74 (m, 2H, —Si—C***H*****$_2$**—CH_2—CH_2—).

Synthesis of Alkyne-functionalized POSS (Alkyne-POSS). As show in Scheme 1, 2-Propynylamine (208 μL, 3.0 mmol) was added to a solution of carboxyl-POSS (2 g, 2.1 mmol) in 15 mL of dichloromethane (CH_2Cl_2) in a flask and was allowed to be dissolved fully under stirring. Then, 1-(3-dimethylaminopropyl)-3-ethylcarbodiimide hydrochloride (EDCI) (0.40 g, 2.1 mmol) and 4-dimethylamiopyridine (DMAP) (0.03 g, 0.25 mmol) were added, and the mixture was stirred at 35°C for 48 h. Afterward, the reaction mixture was washed with water (100 mL) for three times. The organic layer was dried with $MgSO_4$ overnight and the solvent was evaporated under vacuum to yield a 1.89 g of alkyne-POSS. FTIR (KBr, cm^{-1}): 1110 (Si—O—Si), 1529 and 1648 (C=O), 3309 (≡*C*—*H*); ^{1}H-NMR ($CDCl_3$, 400 MHz, δ ppm): 4.11 (d, 2H, —C***H*****$_2$**—C≡CH), 3.23 (d, 2H, —S—C***H*****$_2$**—CO—), 2.58 (t, 2H, —CH_2—C***H*****$_2$**—S—), 2.27 (t, 1H,

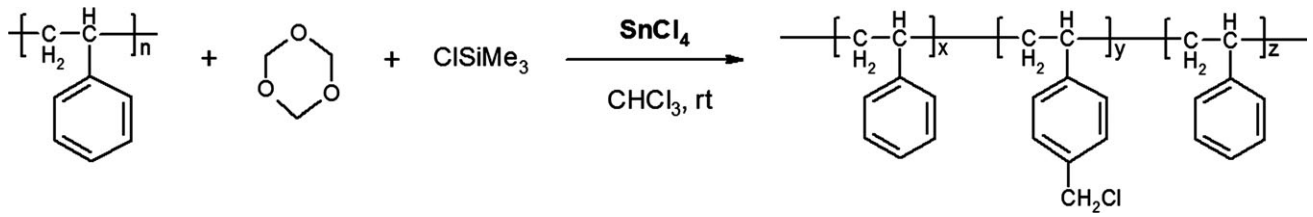

Scheme 2. Chloromethylation of polystyrene.

—C≡C***H***), 1.72 (t, 2H, —Si—CH_2—C***H₂***—CH_2—), 0.74 (m, 2H, —Si—C***H₂***—CH_2—CH_2—).

Synthesis of Chloromethylate PS [PS-$(CH_2Cl)_m$]. The chloromethylation of PS was performed according to the approach suggested by Itsuno et al.,[25] which was originally used for halomethylation of crosslinked PS. A typical procedure is described as follows (Scheme 2). PS (5.0 g), trioxane (3 g, 0.33 mol), and chlorotrimethylsilane (12.7 mL, 98 mmol) were dissolved in 300 mL of chloroform in a flask and were allowed to be fully dissolved under stirring. After the reaction mixture was cooled to 0°C, tin(IV) chloride (0.7 mL, 6 mmol) was added, and the solution was stirred under for 30 min and further at room temperature (25°C) for another several hours. The reaction was quenched by adding 300 mL ethanol. The product was purified by dissolving-precipitation in THF-ethanol for three times, and then dried overnight in a vacuum oven at room temperature. The chloromethylation functionality (F_{-CH_2Cl}) was determined by ^{1}H-NMR characterization according to equation:

$$F_{-CH_2Cl}(\%) = \frac{5A_{-CH_2Cl}}{A_{-CH_2Cl} + 2A_{ben}} \times 100\%,$$

where A_{-CH_2Cl} is the peak area of —CH_2Cl at δ = 4.5 ppm and A_{ben} is the peak area of the benzene ring at δ = 6.5–7.0 ppm.

Synthesis of Azido-Functionalized PS [PS-$(CH_2N_3)_m$]. A typical reaction procedure for azidation of PS-CH_2Cl is described as follows (Scheme 3): 2 g of PS-CH_2Cl and 40 mg of NaN_3 were dissolved in 20 mL of dimethylformamide (DMF) in a flask, and the solution was stirred at room temperature for 24 h. Then, the mixture was precipitated in water to remove unreacted NaN_3 and the final product PS-$(CH_2N_3)_m$ was dried overnight in a vacuum oven at 50°C.

Synthesis of POSS Hybrid PS via Alkyne-azide Click Coupling. Typically, 1 g of PS-CH_2N_3 and alkyne-POSS (0.95 g, 0.96 mmol) was dissolved in 40 mL of DMF in a flask. Copper iodide (CuI) (0.182 g, 0.96 mmol) and PMDETA (201 μL, 0.96 mmol) were added under nitrogen atmosphere. The coupling reaction of the PS-$(CH_2N_3)_m$ and alkyne-POSS was carried out at 25°C for 24 h via Cu (I)-catalyzed click chemistry (Scheme 4). Afterward, the reaction mixture was passed through a basic alumina column. And the concentrated solution was precipitated in methanol and further purified. The resulting product was dried overnight under vacuum at 50°C, and yields a 1.81 g of hybrid PS-*g*-POSS.

Characterization

FTIR spectroscopic measurements were performed using a NEXUS 6700 device (Thermo-Nicolet, Inc., USA) at room temperature (25°C) in the range of 4000–400 cm^{-1} at a resolution of 1.0 cm^{-1}. All samples were scrawled on KBr flakes for FTIR measurements.

The nuclear magnetic resonance spectroscopy (^{1}H-NMR) was recorded on samples dissolved in $CDCl_3$ with a Bruker AV600 MHz spectrometer (USA) at 25°C. Chemical shifts were referenced to tetramethylsilane.

The number-average molecular weight (M_n), weight molecular weight (M_w), and molecular weight distribution (MWD, M_w/M_n) were determined by a Waters 515–2410 Gel permeation chromatograph (GPC, Waters, USA). THF served as solvent of samples with the concentration of 20 mg polymer per 10 mL of THF and

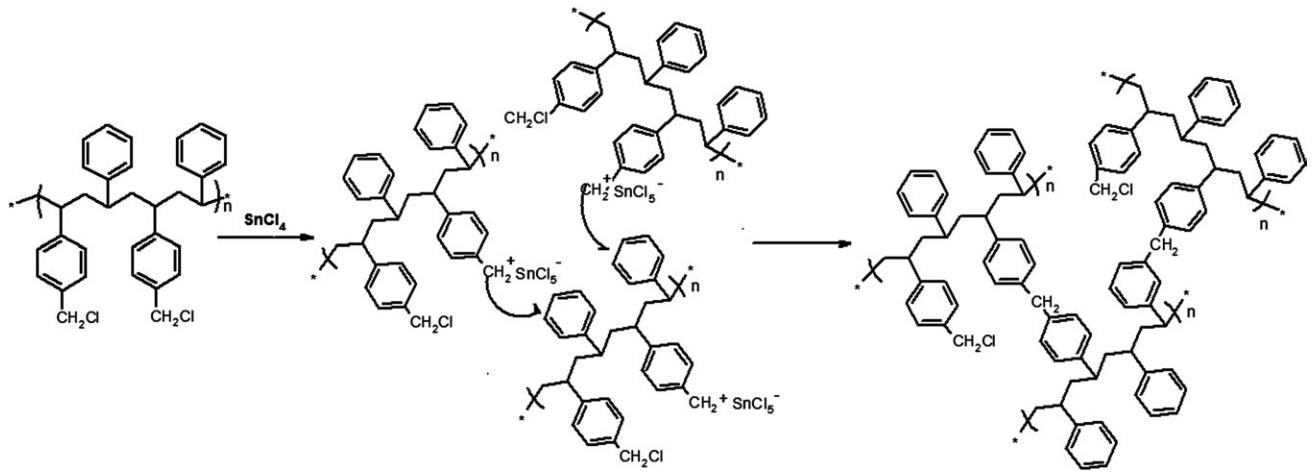

Scheme 3. The mechanism of the crosslink reaction.

Applied Polymer SCIENCE

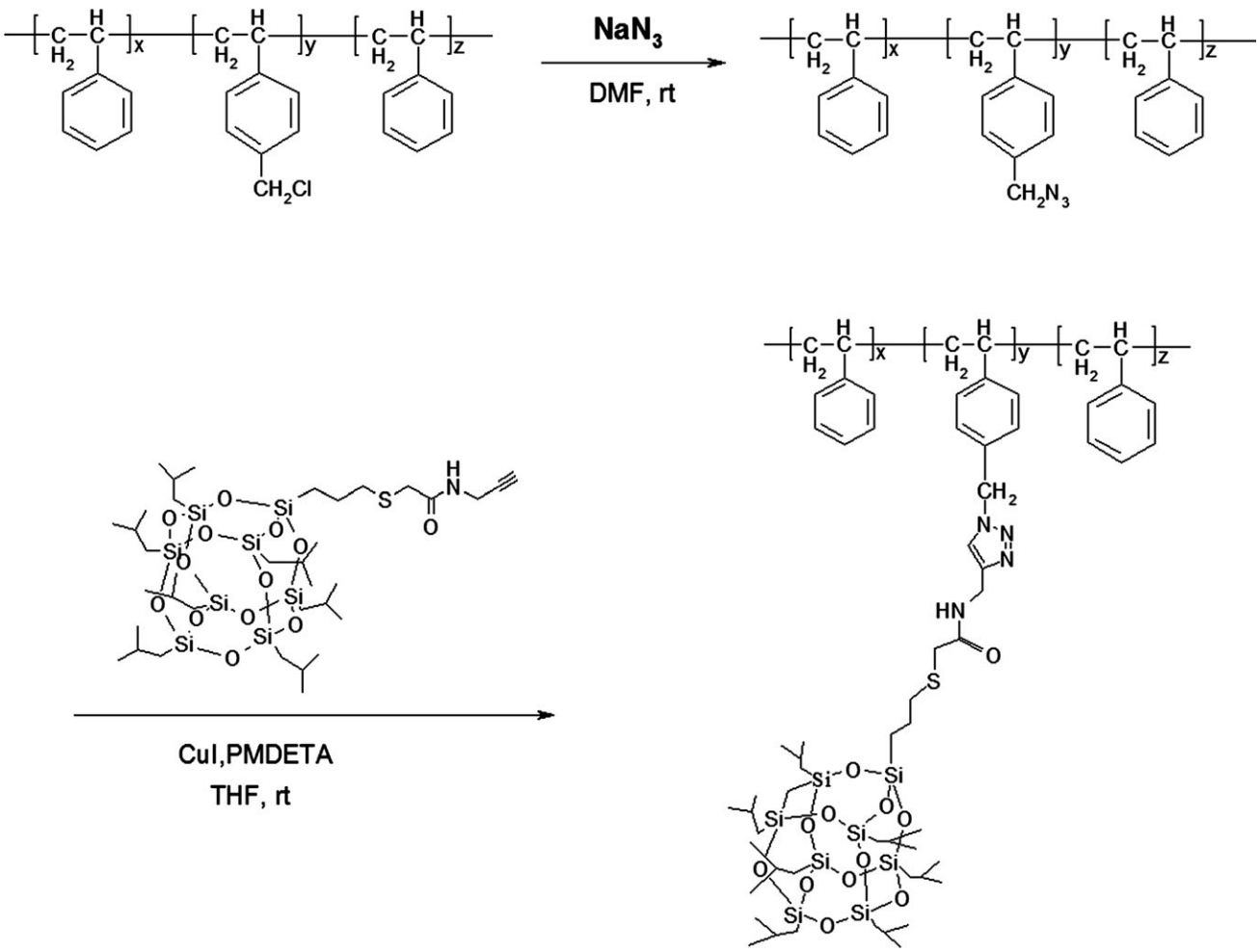

Scheme 4. Synthesis of PS-*g*-POSS via click coupling.

the mobile phase at a flow rate of 1.0 mL/min. PS standards with narrow molecular weight distribution were used for the calibration.

Surface static contact angles were performed and detected on a Dataphysics OCA-20 (Dataphysics Inc., GmbH, Germany) with 5 μL of distilled water droplet being placed on the treated film by a micro-syringe and observed through a traveling microscope fitted with a goniometer eyepiece; all measurements were performed at 25°C and were the average of at least six readings at different positions across the surface.

The calorimetric measurements were performed on a Q200 (TA Instruments Company) differential scanning calorimeter (DSC) in a dry nitrogen atmosphere. The instrument was calibrated with standard indium. All the samples were heated to 200°C, isothermal for 5 min, then cooling to 25°C, and DSC curves were recorded at a heating rate of 10°C/min. The glass–transition temperatures (T_g) were taken as the midpoint of the capacity change.

Transmission electron microscopy (TEM) measurements were performed on a H-800 electron microscope (Hitachi, Japan) operating at an acceleration voltage of 200 KV. The samples for TEM observation were prepared by spreading a drop of aggregate solution (0.2 wt %) on a copper grid (400 meshes) coated with a carbon film or lacey support films, followed by air drying at 25°C before the measurement.

A wide-angle X-ray diffraction (XRD) study of the samples was performed on a Bruker D8 X-ray diffractometer (Bruker Co., Germany) with Cu Kα radiation at 1.540 Å in the range of $5° \leq 2\theta \leq 50°$at a scanning rate of 5°/min.

Mechanical properties were measured on Instron-1185 instrument universal testing machine (Instron Co., UK) with the tensile rate at 10 mm/min at 25°C. The GPPS/PS-*g*-POSS composites were blended through a Dynisco Laboratory Mixing Extruder (LME-230, Dynisco, USA) at 185°C. The tensile samples were made using a Dynisco Laboratory Mixing Molder (LMM-4-230, Dynisco, USA) in accordance with the ASTM D1708 standard.

Examination of the fracture surface of tensile specimen was performed on a Zeiss Supra 55 scanning electron microscope (SEM). The fracture ends were cut off and mounted on the aluminum stubs, then coated with a thin layer of gold.

RESULTS AND DISCUSSION

Chloromethylation of PS

The usual chloromethylation of PS by using chloromethyl methyl ether or bis(chloromethyl) ether as chlorine

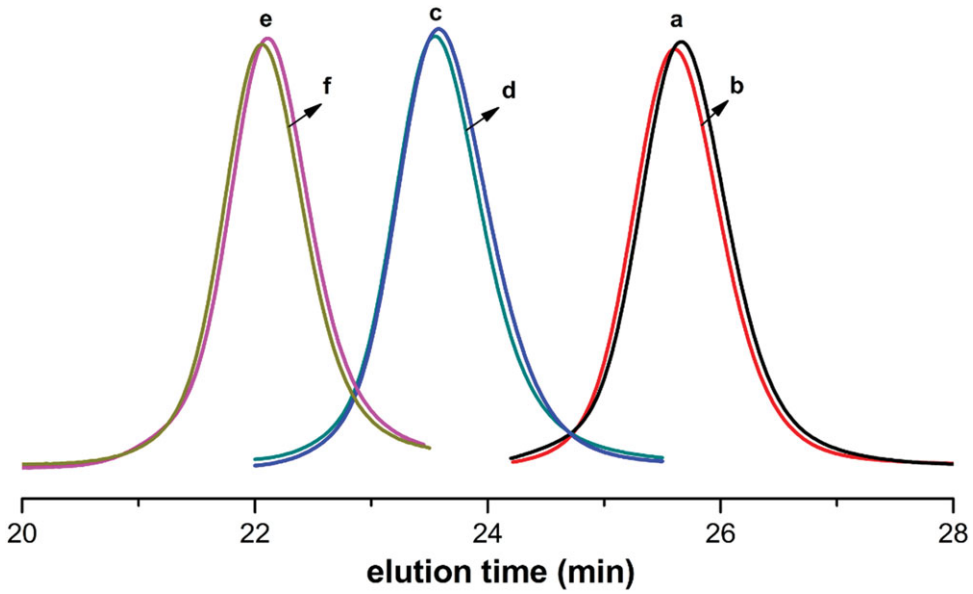

Figure 1. GPC profiles of (a) PS-13k, (b) PS-$(CH_2Cl)_m$-13k (M_n = 13k, PDI = 1.1, F_{-CH_2Cl} = 10 mol %), (c) PS-38k, (d) PS-$(CH_2Cl)_m$-38k (M_n = 39k, PDI = 1.1, F_{-CH_2Cl} = 9 mol %), (e) PS-110k, (f) PS-$(CH_2Cl)_m$-110k (M_n = 110k, PDI = 1.1, F_{-CH_2Cl} = 11 mol %). [Color figure can be viewed in the online issue, which is available at wileyonlinelibrary.com.]

methylation reagent has been applied for a variety of preparations of reactive PSs, but the these reagents are potential carcinogens. Several alternative procedures to chloromethylated PS have been suggested, but it has been noted that the level of substitution is difficult to control due to alkylation among intermolecular chains, as shown in Scheme 3.[26,27] In this article, the chloromethylation of PS was performed with trioxane and chlorotrimethylsilane as chlorine methylation reagent according to the approach suggested by Itsuno et al.[25] (Scheme 2). In order to investigate the controlled chloromethylation of PS, PS with different M_n of 13 × 103, 38 × 103, and 110 × 103 g/mol were reacted. The results in Figure 1 proved that

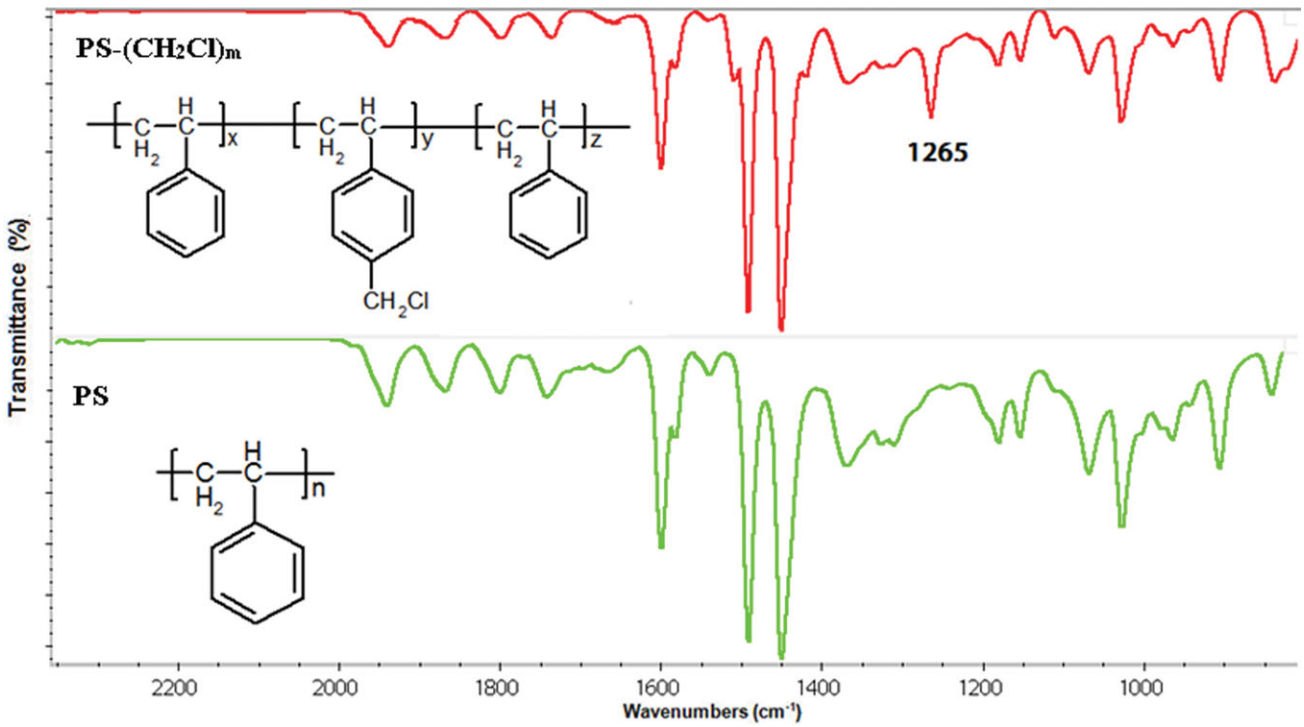

Figure 2. FTIR and spectra of GPPS and PS-$(CH_2Cl)_m$, F_{-CH_2Cl}= 10 mol %). [Color figure can be viewed in the online issue, which is available at wileyonlinelibrary.com.]

Applied Polymer SCIENCE

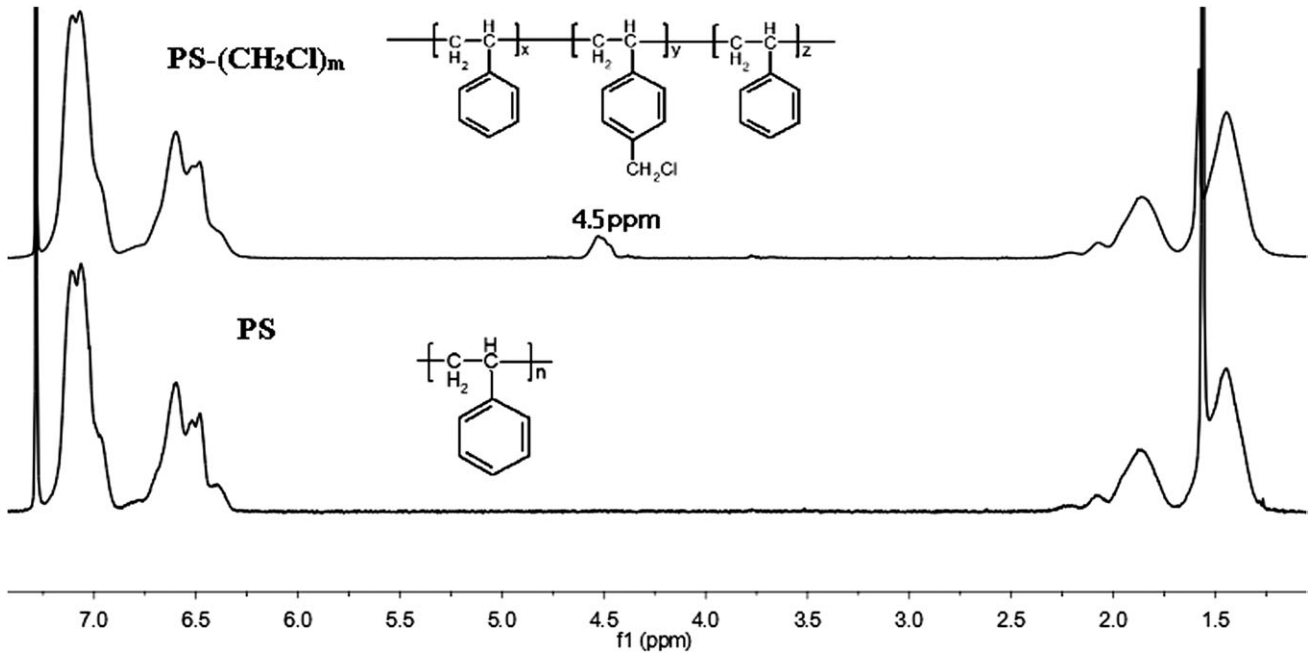

Figure 3. ^{1}H NMR spectra of GPPS and PS-$(CH_2Cl)_m$, F_{-CH_2Cl}= 10 mol%).

PS with different molecular weight has a similar F_{-CH_2Cl} under the same chloromethylation condition at room temperature (25°C) for 3 h. GPC traces of PS and PS-$(CH_2Cl)_m$ show a perfect symmetric molecular weight distribution before and after chloromethylation. The molecular weight of PS-$(CH_2Cl)_m$ slightly increased. Therefore, the side alkylation reaction to form crosslinking chloromethylated PS could be suppressed by using chloroform as solvent under relatively low concentration of $SnCl_4$ at low temperature.

On the basis of the above optimized reaction conditions for chloromethylation, the effect of reaction time on chloromethylation functionality was further investigated, and the results are shown in Figure 4. The FTIR and ^{1}H-NMR spectra of PS-$(CH_2Cl)_m$ are given in Figures 2 and 3, respectively. The obvious characteristic peak at 1265 cm^{-1} due to C—]Cl stretching in —CH_2Cl groups indicates the successful chloromethylation and formation of PS-$(CH_2Cl)_m$. The ^{1}H-NMR spectrum of PS-CH_2Cl in Figure 3 displays a new characteristic resonance at

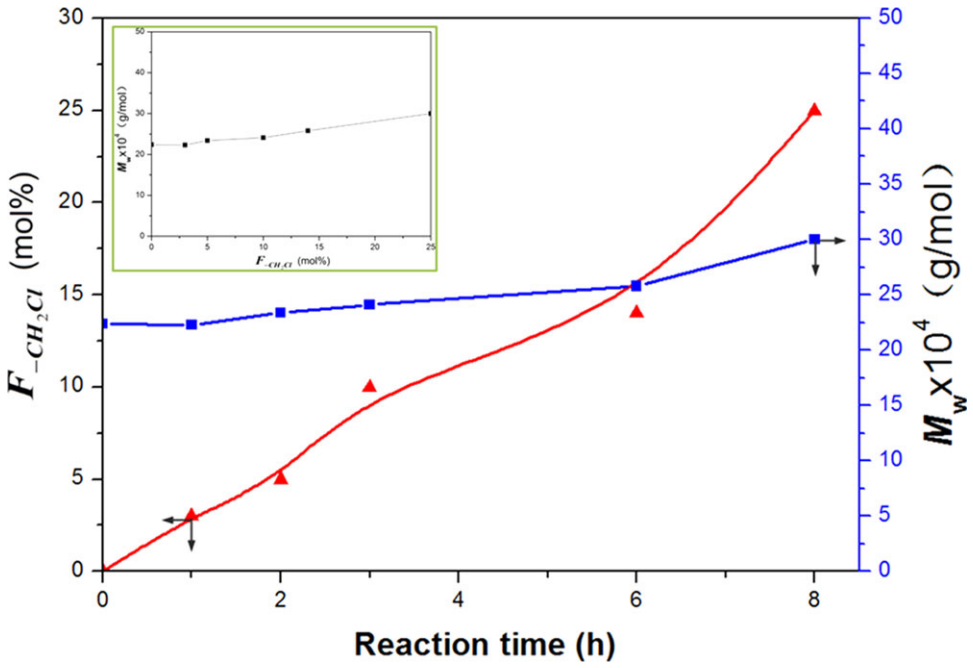

Figure 4. The chloromethylation functionality and M_w of GPPS and PS-$(CH_2Cl)_m$. [Color figure can be viewed in the online issue, which is available at wileyonlinelibrary.com.]

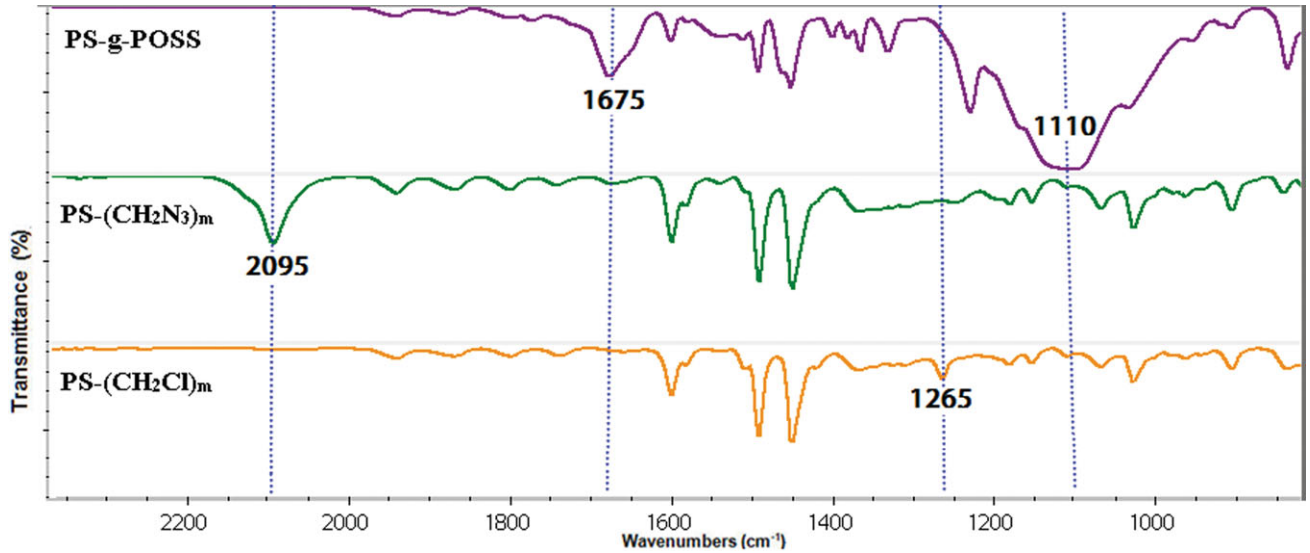

Figure 5. FTIR spectra of PS, PS-$(CH_2Cl)_m$, PS-$(CH_2N_3)_m$, and PS-*g*-POSS (F_{-CH_2Cl}=10 mol %). [Color figure can be viewed in the online issue, which is available at wileyonlinelibrary.com.]

4.5 ppm, corresponding to the proton in —C**H**$_2$Cl groups, which further confirms the chloromethylation of PS at the phenyl ring.

It can be seen from Figure 4 that F_{-CH_2Cl} increased obviously from 0 to 25% with chloromethylation times. While M_w almost kept unchanged from 22.4 to 25.8 $\times$ 10^4 with increasing F_{-CH_2Cl} from 0 to 14% and slightly increased with further increasing F_{-CH_2Cl} to 25% due to a small amount of intermolecular alkylation.

Synthesis and Characterization of PS-*g*-POSS via Click Coupling Reaction. Azido-functionalized PS [PS-$(CH_2N_3)_m$] was obtained by means of azidation of PS-CH_2Cl via simple reaction of sodium azide (Scheme 4).

The FTIR spectra of PS-$(CH_2Cl)_m$ and PS-$(CH_2N_3)_m$ and covalent functionalization of PS with POSS are shown in Figure 5. Compared to PS-$(CH_2Cl)_m$, the peak at 1265 cm^{-1} for C—Cl stretching in PS-$(CH_2Cl)_m$ disappeared completely and the absorption at 2095 cm^{-1} ascribed to the azide group appeared

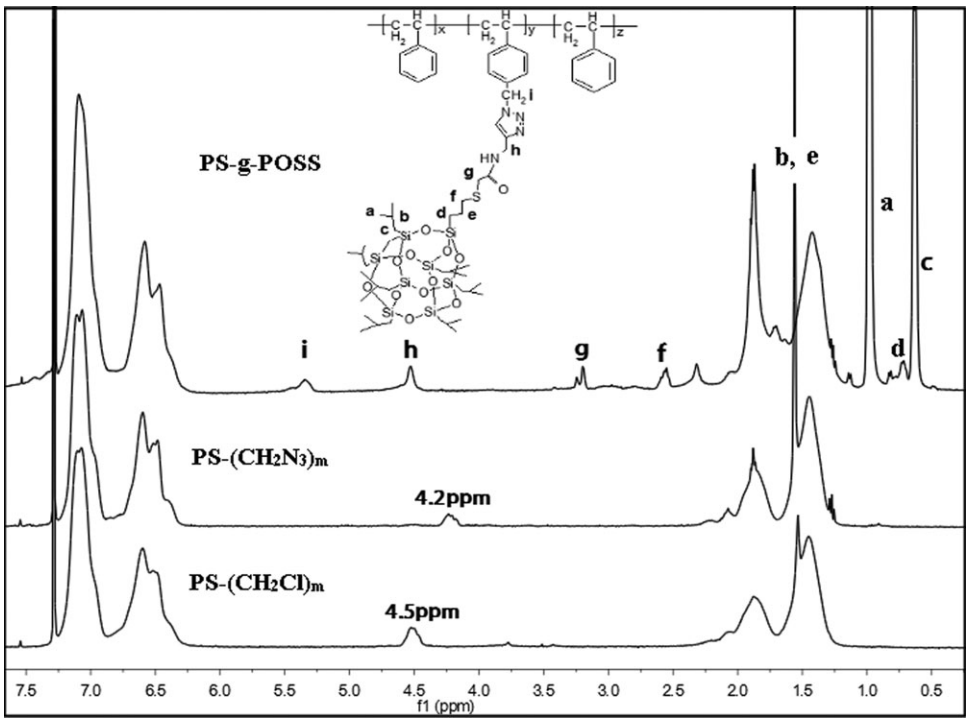

Figure 6. ^{1}H NMR spectra of PS-$(CH_2Cl)_m$, PS-$(CH_2N_3)_m$, and PS-*g*-POSS (F_{-CH_2Cl}=10 mol %).

Applied Polymer SCIENCE

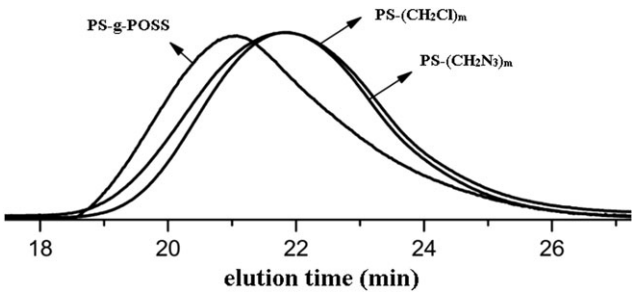

Figure 7. GPC profiles of PS-$(CH_2Cl)_m$ (M_n = 96k, PDI = 2.5), PS-$(CH_2N_3)_m$ (M_n = 90k, PDI = 2.5), and PS-*g*-POSS (M_n = 150k, PDI = 3.1, F_{-CH_2Cl} = 10 mol %).

presented after reaction with NaN_3 in DMF at room temperature. When PS-$(CH_2N_3)_m$ further reacted with alkyne-POSS, the band at 2095 cm^{-1} disappeared completely after alkyne-azide coupling reaction, and a strong absorption at 1110 cm^{-1} assigned to Si—O—Si stretching from POSS appeared correspondingly. Besides, the peak at 1675 cm^{-1}, which is ascribed to the formation of triazole ring, provides a fairly intuitive evidence for the success of coupling reaction. Likewise, the ^1H NMR spectrum of PS-CH_2Cl shown in Figure 6 displays a characteristic resonance at 4.5 ppm, corresponding to the proton in —CH_2Cl, and it can be observed from the spectrum of PS-C***H₂***N_3, the characteristic signal at 4.5 ppm of PS-CH_2Cl was completely shifted to 4.2 ppm assigned to the protons of —C***H₂***N_3 after azidation reaction. Therefore, due to the efficient conversion of azidation, azidation functionality ($F_{-CH_2N_3}$) of PS-$(CH_2N_3)_m$ is consistent with F_{-CH_2Cl}, which is similar to those by FTIR characterization. Compared to ^1H NMR spectrum of PS-$(CH_2N_3)_m$, it can be seen from ^1H NMR spectrum of PS-*g*-POSS shown in Figure 6 that the alkyne-azide cycloaddition occurred with extremely high efficiency due to complete disappearance of resonance of the azide group at 4.2 ppm. Besides, the characteristic signal at 0.62 ppm (peak c) assigned to the protons in —C***H₂***— generated from seven isobutyl groups of POSS. The chemical shifts in the range from 0.8 to 2.1 ppm are corresponding to the protons in backbone of PS and the methyl and methine protons of POSS, respectively. Moreover, the presence of characteristic signals at 4.55 ppm (peak h) and 5.38 ppm (peak i) are assigned to the proton in —C***H₂***— adjacent to the triazole ring, by which the alkyne-azide click reactions were confirmed. The GPC traces of PS-CH_2Cl, PS-CH_2N_3, and PS-*g*-POSS are shown in Figure 7. In contrast to GPC curves of PS-*g*-POSS, PS-CH_2Cl, and PS-CH_2N_3, an obvious shift toward high molecular weight was observed, and the coupling reaction between azido-functionalized PS and alkyne-POSS was confirmed.

The surface property of polymer incorporated POSS could be influenced due to low surface energy of cage-like nanostructure of POSS.[15] The surface energy and wettability of PS-*g*-POSS were further investigated by static contact angle test shown in Figure 8. Compared to the water contact angle of 85° for GPPS, PS-*g*-POSS-10% and PS-*g*-POSS-25% have an increased contact angle to 98° and 113°, respectively, which show a better hydrophobic property of PS-*g*-POSS surface than that of neat PS. The results indicate that POSS plays an important role to lower the surface free energy in hybrid materials.

The grafting architecture leads to changes in movement of segment in PS-*g*-POSS hybrid copolymers. The effect of grafting degree on T_g of PS and PS-*g*-POSS is shown in Figure 9. It can be clearly seen that T_g of PS-*g*-POSS was lower than that of PS when grafting degree was lower than 5%, while T_g of PS-*g*-POSS with 10% or 25% of grafting degree was higher than that of PS. The lower T_g of PS-*g*-POSS with $\leq$5% of grafting degree was attributed to the easier movement of PS segments caused by the increase in free volume and decrease in rotational energy barriers, which is similar to the report by P. T. Mather, *et al.*[17] The T_g increased upto 112°C with increasing grafting degree to 25% due to the increase in rigid side POSS groups and intermolecular interactions between POSS groups.

Micromorphology of PS-*g*-POSS. To further elucidate the micromorphology of PS-*g*-POSS hybrid polymers, the transmission electron microscopy (TEM) images of PS/POSS (50/50 wt %) blends and PS-*g*-POSS hybrid copolymers without staining are shown in Figure 10. It can be observed from Figure 10(a) that POSS aggregated with 250–500 nm in size in PS/POSS blends, which is similar to the reports such as POSS blended with polymethyl methacrylate (PMMA)[28] and phenolic resins.[29]

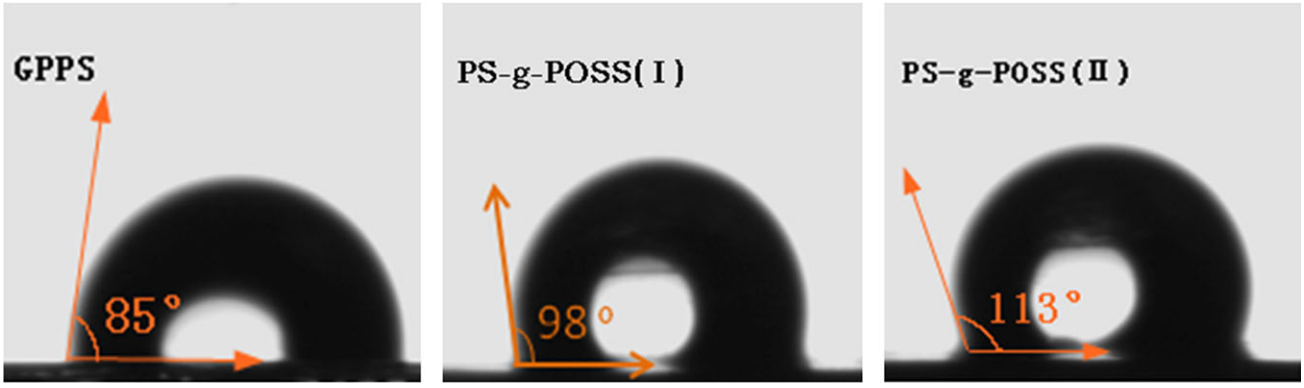

Figure 8. Water contact angles images of GPPS and PS-*g*-POSS (I,F_{-CH_2Cl} = 10 mol % and II, F_{-CH_2Cl} = 25 mol %). [Color figure can be viewed in the online issue, which is available at wileyonlinelibrary.com.]

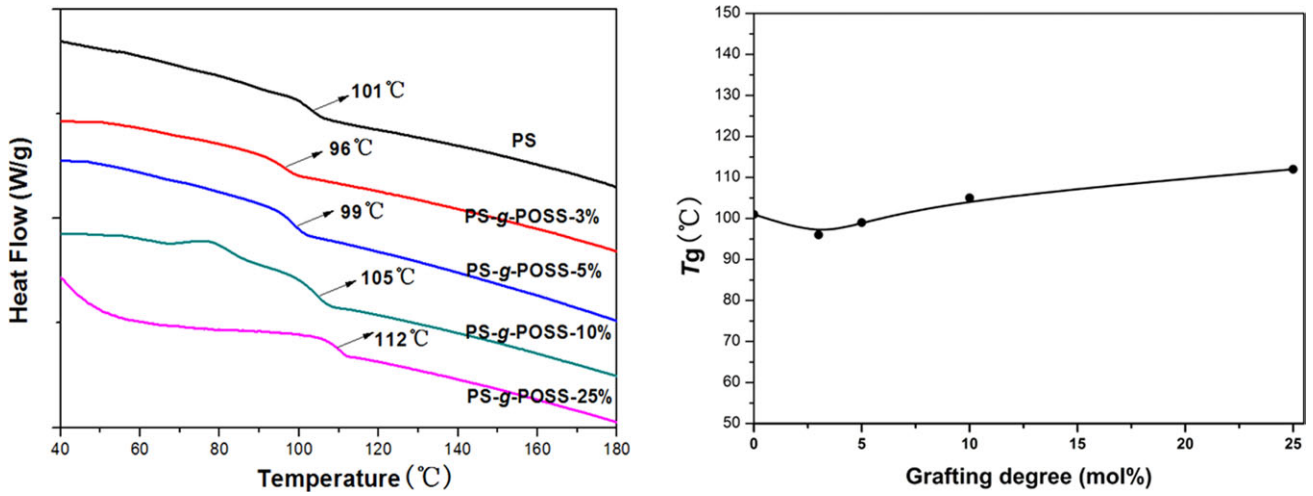

Figure 9. The DSC curves of the GPPS and PS-*g*-POSS. [Color figure can be viewed in the online issue, which is available at wileyonlinelibrary.com.]

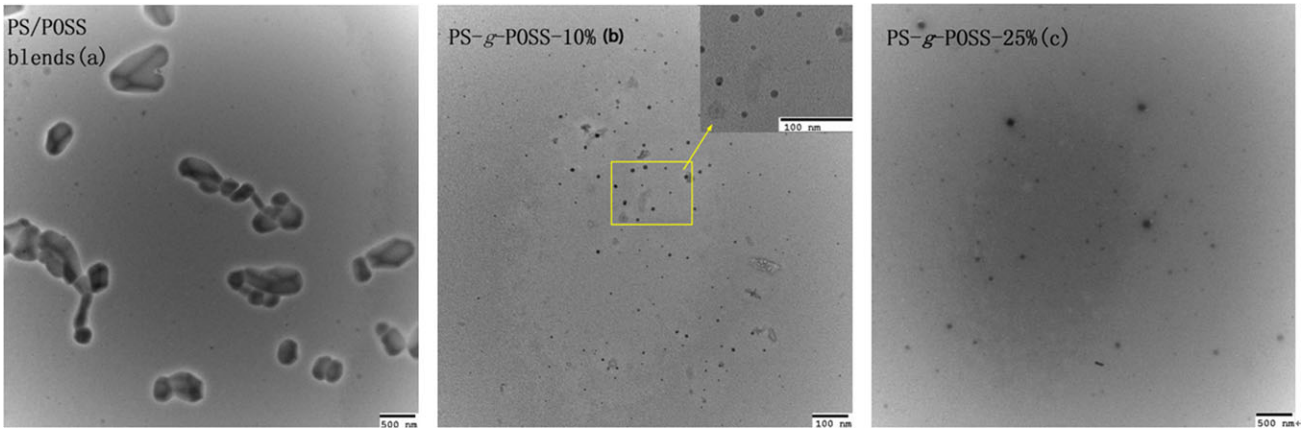

Figure 10. TEM images of PS/POSS blends (a) and PS-*g*-POSS [F_{-CH_2Cl} = 10mol % (b), F_{-CH_2Cl} = 25 mol % (c)]. [Color figure can be viewed in the online issue, which is available at wileyonlinelibrary.com.]

Interestingly, the TEM images of PS-*g*-POSS with 10% and 25% of grafting degree [about 50 wt % and 70 wt %, respectively; Figure 10(b)] show a well-dispersed organization of small-sized self-assemble behavior, and self-aggregate part with average diameter of around 10 nm in size (black) originating from POSS in PS matrix, which is similar to the report on PS-POSS copolymers.[30] Further increase in POSS concentration leads to the increase of particle size shown in Figure 10(c), the various sizes are even to near to 80 nm. These results would provide us a micro-view that how POSS–polymer interactions take effect in variety of performance aspects.

The XRD patterns of PS-*g*-POSS should exhibit aggregates reflections of POSS if they are well dispersed in the matrix. Figure 11 shows XRD patterns of alkyne-POSS, PS, and PS-*g*-POSS hybrid copolymers with different grafting degree. The neat PS shows an amorphous peak at $2\theta = 19°$. For comparison, others showed a distinct new peak ($2\theta = 8.3°$) due to the POSS molecules. Besides, the peak height of POSS increased with POSS concentration in PS-*g*-POSS, which displays a similar morphology in many POSS-polymer materials.[31,32] Consistent with our

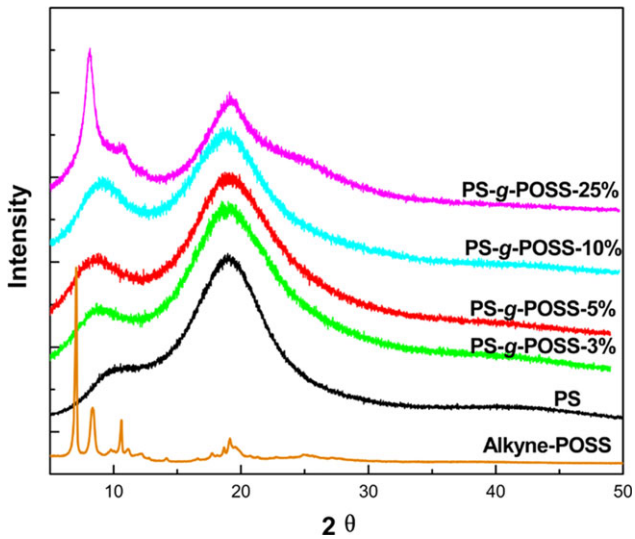

Figure 11. X-Ray diffraction of alkyne-POSS, PS and PS-*g*-POSS products. [Color figure can be viewed in the online issue, which is available at wileyonlinelibrary.com.]

Applied Polymer SCIENCE

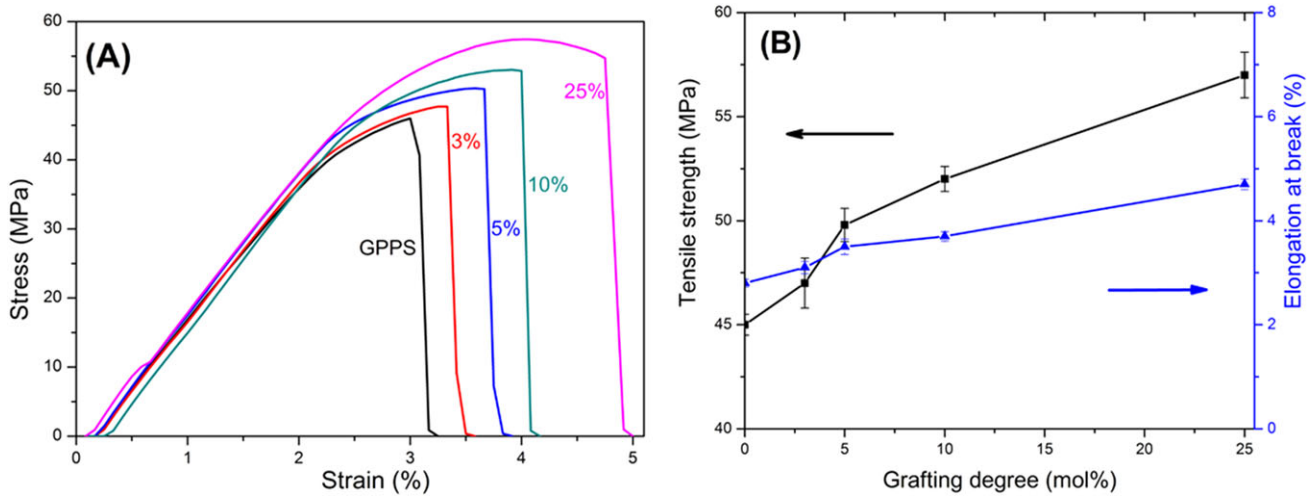

Figure 12. (A) Stress–strain curves of GPPS and GPPS/5 wt %PS-*g*-POSS and (B) Tensile strength and elongation at break of GPPS/5 wt % PS-*g*-POSS. [Color figure can be viewed in the online issue, which is available at wileyonlinelibrary.com.]

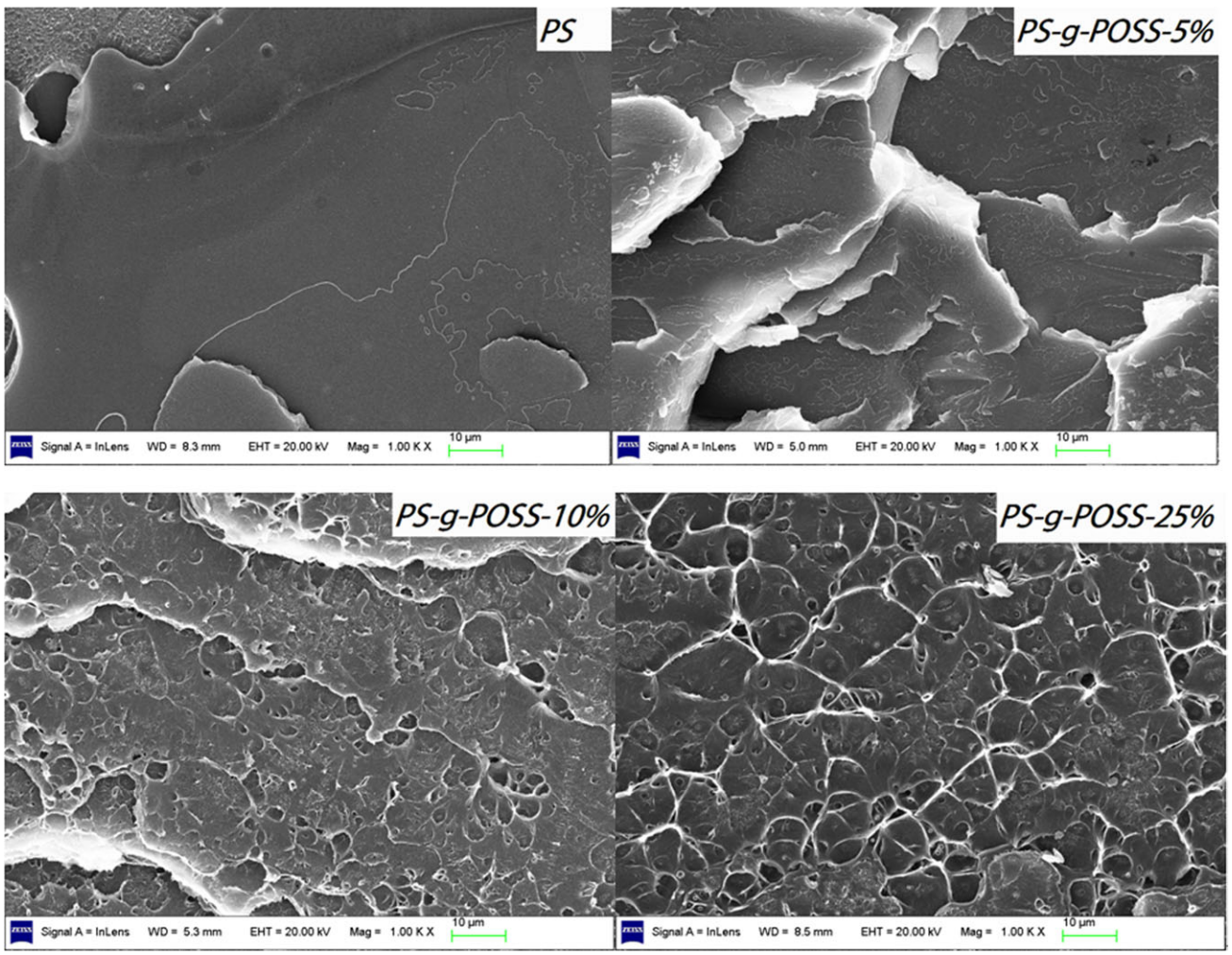

Figure 13. SEM micrographs of the tensile fracture surface of GPPS and GPPS/5 wt % PS-*g*-POSS. [Color figure can be viewed in the online issue, which is available at wileyonlinelibrary.com.]

TEM observations described above, XRD curve of PS-*g*-POSS-25% shows a sharp peak corresponding to the POSS aggregates.

Mechanical Analysis of PS-*g*-POSS. The hard core with Si—O—Si inorganic structure would provide a unique mechanical property of POSS hybrid polymer materials. As our previous work,[9] GPPS could be greatly toughened by introduction of a small amount of *cis*-SB, the tensile strength, and elongation at break could also be increased due to the nanometer-scale rubber phases and some partially crystalline PS segments in the *cis*-SB block copolymer. Herein, we try to use these PS-*g*-POSS hybrid materials to reinforce the GPPS. Stress–strain curves of GPPS and GPPS/5 wt % PS-*g*-POSS with different POSS contents are shown in Figure 12(A). Compared to a parallel PS sample, the tensile strength of GPPS/PS-*g*-POSS composites increased greatly with increasing grafting degree of PS-*g*-POSS from 45 to 57 MPa [Figure 12(B)]. The physical property could be remarkably increased by 27% with introducing 5% of PS-*g*-POSS hybrid copolymers, which is attributed to the nano-POSS aggregate phase in PS matrix to resist tensile deformation. As a result of these mechanical properties, PS-*g*-POSS have a remarkable increasing in tensile strength and elongation at break, which would be a significant in the application of PS materials.

The SEM images of the tensile fracture surface of GPPS and GPPS/5 wt % PS-*g*-POSS with different POSS contents are shown in Figure 13. It can be seen from SEM images that the tensile fracture surface of GPPS specimen was relatively smooth and a brittle fracture feature was presented, while those of GPPS/5 wt % PS-*g*-POSS blends become more and more rough and coarse, which can absorb part of the energy when break happens. Some similar phenomena also have been studied in other POSS hybrid polymers system.[11,33]

CONCLUSIONS

A novel PS-*g*-POSS organic–inorganic hybrid graft copolymer could be successfully prepared via Cu(I)-catalyzed 1,3-dipolarcycloaddition between mono-functional alkyne-POSS and multi-functional azido-PS. Alkyne-functionalized POSS was synthesized with very high yield by thiol-ene facile click reaction and subsequent amidation reaction. Azido-functionalized PS were synthesized by cholromethylation and subsequent azido reaction with full conversion, and the results show PS with different molecular weight has a similar F_{-CH_2Cl} under the same chloromethylation condition and cross-linking reaction could be effectively suppressed under the chloromethylation functionality of 25 mol%. PS-*g*-POSS presented a better hydrophobic property with contact angle of 113° than that of PS (85°). T_g of PS-*g*-POSS was decreased from the 101°C of GPPS to 96°C of PS-*g*-POSS with 3 mol% POSS due to addition of free volume, then T_g increased gradually to 112°C with 25 mol% POSS because of the steric effect and intermolecular interactions. An obvious aggregation of POSS inorganic phase of around 10–80 nm in size formed to PS-*g*-POSS matrix. In addition, 5 wt % of PS-*g*-POSS was added to GPPS to remarkably improve the tensile strength from 45 to 57 MPa. SEM images show that the fracture surfaces of PS/PS-*g*-POSS composites become more and more coarse which can absorb part of the energy when break happens to enhance the mechanical properties of polymers.

ACKNOWLEDGMENTS

The financial supports from National Natural Science Foundation of China (50873009 and 51173011) are greatly appreciated.

REFERENCES

1. Li, S. H.; Lin, M. M.; Toprak, M. S.; Kim, D. K.; Muhammed, M. *Nano Rev.* **2010**, *1*, 1.
2. Gomez-Romero, P. *Adv. Mater.* **2001**, *13*, 163.
3. Chen, Q.; Xu, R. W.; Zhang, J.; Yu, D. S. *Macromol. Rapid Commun.* **2005**, *26*, 1878.
4. Zhang, Y. D.; Lee, S. H.; Yoonessic, M.; Liang, K. W.; Pittman, C. U. *Polymer* **2006**, *47*(9), 2984.
5. Fina, A.; Bocchini, S.; Camino, G. *Polym. Degrad. Stab.* **2008**, *93*(9), 1647.
6. Hosaka, N.; Torikai, N.; Otsuka, H.; Takahara, A. *Langmuir* **2007**, *23*(2), 902.
7. Hirai, T.; Leolukman, M.; Jin, S.; Goseki, R.; Ishida, Y.; Kakimoto, M.; Hayakawa, T.; Ree, M.; Gopalan, P. *Macromolecules* **2009**, *42*, 8835.
8. Wei, J.; Tan, B. H.; Bai, Y.; Ma, J.; Lu, X. H. *J. Phys. Chem. B* **2011**, *115*, 1929.
9. Zhu, H.; Wu, Y. X.; Zhao, J. W.; Xu, R. W.; Huang, Q. G.; Wu, G. Y. *Macromol. Symp.* **2008**, *261*, 130.
10. Liu, L.; Hu, Y.; Song, L.; Nazare, S.; He, S. Q.; Hull, R. *J. Mater. Sci.* **2007**, *42*, 4325.
11. Dintcheva1, N. Tz.; Morici, E.; Arrigo, R.; La, Mantia. F. P.; Malatesta, V.; Schwab, J. J. *eXPRESS Polym. Lett.* **2012**, *6*, 561.
12. Voronkov, M. G.; Lavrent'yev, V. I. *Top. Curr. Chem.* **1982**, *102*, 199.
13. Shockey, E. G.; Bolf, A. G.; Jones, P. F.; Schwab, J. J.; Chaffee, K. P.; Haddad, T. S.; Lichtenhan, J. D. *Appl. Organometal. Chem.* **1999**, *13*, 311.
14. Haddad, T. S.; Lichtenhan, J. D. *Macromolecules* **1996**, *29*, 7302.
15. Misra, R.; Fu, B. X.; Morgan, S. E. *J. Polym. Sci. Part B: Polym. Phys.* **2007**, *45*, 2441.
16. Carroll, J. B., Waddon, A. J., Nakade, H.; Rotello, V. M. *Macromolecules* **2006**, *36*, 6289.
17. Wu, J., Haddad, T. S.; Mather, P. T. *Macromolecules* **2009**, *42*, 1142.
18. Zhang, H. X., Lee, H. Y., Shin, Y. J., Yoon, K. B., Noh, S. K.; Lee, D. H. *Polym. Int.* **2008**, *57*, 1351.
19. Kolb, H. C., Finn, M. G.; Sharpless, K. B. *Angew. Chem. Int. Ed.* **2001**, *40*, 2004.
20. Barner-Kowollik, C., DuPrez, F. E., Espeel, P., Hawker, C. J., Junkers, T., Schlaad, H.; Van Camp, W. *Angew. Chem. Int. Ed.* **2011**, *50*, 60.
21. Petraru, L.; Binder, W. H. *Polym. Prepr.* **2005**, *46*, 841.
22. Trastoy, B., Pérez-Ojeda, M. E.; Sastre, R. *Chem. Eur. J.* **2010**, *6*, 3833.

23. Cordes, D. B.; Lickiss, P. D.; Ratabou, F. *Chem. Rev.* **2010**, *110*, 2081.
24. Zhang, W. A.; Müller, A. H. E. *Macromolecules* **2010**, *43*, 3148.
25. Itsuno, S.; Uchikoshi, K.; Ito, K. *J. Am. Chem. Soc.* **1990**, *112*, 8187.
26. Wright, M. E.; Toplikar, E. G.; Svejda, S. A. *Macromolecules* **1991**, *24*, 5879.
27. Moulay, S.; Mehdi, N. *Chin. J. Polym. Sci.* **2006**, *24*, 627.
28. Weickmann, H.; Delto, R.; Thomann, R.; Brenn, R.; Döll, W.; Koh, K.; Mülhaupt, R. *J. Mater. Sci.* **2007**, *42*, 87.
29. Zhang, Y. D.; Lee, S.; Yoonessi, M.; Liang, K. W.; Pittman, C. U. *Polymer* **2006**, *47*, 2984.
30. Wu, J.; Haddad, T. S.; Kim, G. Y.; Mather, P. T. *Macromolecules* **2007**, *40*, 544.
31. Zheng, L.; Waddon, A. J.; Farris, R. J.; Coughlin, E. B. *Macromolecules* **2002**, *35*, 2375.
32. Song, X. Y.; Geng, H. P.; Li, Q. F. *Polymer* **2006**, *47*, 3049.
33. Zhang, Z. P.; Gu, A. J.; Liang, G. Z.; Ren, P. G.; Xie, J. Q.; Wang, X. L. *Polym. Degrad. Stab.* **2007**, *92*, 1986.